Clim Dyn (2009) 33:365–381
DOI 10.1007/s00382-008-0496-1

Impact of transient freshwater releases in the Southern Ocean on the AMOC and climate

Didier Swingedouw · T. Fichefet · H. Goosse · M. F. Loutre

Received: 27 February 2008 / Accepted: 17 November 2008 / Published online: 9 December 2008
© Springer-Verlag 2008

Abstract The bipolar ocean seesaw is a process that explains the competition between deep waters formed in the North Atlantic (NA) and in the Southern Ocean (SO). In this picture, an increase in the rate of formation of one of these water masses is made at the expense of the other. However, recent studies have questioned the effectiveness of this process. Namely, they show that adding freshwater in the SO can reduce deep water formation in the SO as well as in the NA. In this study, we explore the mechanisms and time scales excited by such a SO freshwater release by performing sensitivity experiments where a freshwater input is added abruptly in the ocean, south of 60°S, with different rates and durations. For this purpose, we evaluate the separate effects of wind, temperature and salinity changes, and we put the emphasis on the time evolution of the system. We find three main processes that respond to these freshwater inputs and affect the NA Deep Water (NADW) production: (i) the deep water adjustment, which enhances the NADW cell, (ii) the salinity anomaly spread from the SO, which weakens the NADW cell, and (iii) the increase in the Southern Hemisphere wind stress, which enhances the NADW cell. We show that process (i) affects the Atlantic in a few years, due to an adjustment of the pycnocline depth through oceanic waves in response to the buoyancy perturbation in the SO. The salinity anomalies responsible for the NADW production decrease [process (ii)] invades the NA in around 30 years, while the wind stress from process (iii) increases in around 20 years after the beginning of the freshwater perturbation. Finally, by testing the response of the ocean to a large range of freshwater release fluxes, we show that for fluxes larger than 0.2 Sv, process (ii) dominates over the others and limits NADW production after a few centuries, while for fluxes lower than 0.2 Sv, process (ii) hardly affects the NADW production. On the opposite, the NADW export is increased by processes (i) and (iii) even for fluxes smaller than 0.1 Sv. The climatic impact of the freshwater release in the SO is mainly a cooling of the Southern Hemisphere, of up to 10°C regionally, which increases with freshwater release fluxes for a large range of values.

Keywords Bipolar ocean seesaw · Thermohaline circulation · Southern Ocean · Ocean–climate interactions · Climate variability · Glacial meltwater · Climate modelling

D. Swingedouw (✉) · T. Fichefet · H. Goosse · M. F. Loutre
Institut d'Astronomie et de Géophysique Georges Lemaître, Université Catholique de Louvain, 2 chemin du Cyclotron, 1348 Louvain-la-Neuve, Belgium
e-mail: swingedo@cerfacs.fr

D. Swingedouw
CERFACS/GlobC, 42 Avenue G Coriolis, 31057 Toulouse, France

1 Introduction

Proxy data show an intriguing relationship between the reconstructed temperatures in Greenland and Antarctica. It appears during around the last million years that abrupt cooling periods in Greenland approximately corresponds to slow warming periods in Antarctica (Blunier and Brook 2001; EPICA Community Members 2006). This relationship has been summarised by the so-called bipolar climate seesaw (BCS), an image illustrating the communication between the climate from the Northern and Southern Hemispheres. Several theories have tried to explain the mechanisms leading to this BCS. Most of these explanations involves ocean dynamics, and more particularly the

thermohaline circulation, but differ in the details of the involved mechanisms and timing. A first hypothesis (Crowley 1992) is related to the Atlantic Meridional Overturning Circulation (AMOC), whose weakening can reduce the related northward cross-equatorial heat transport, leading to a BCS pattern. Another explanation (Broecker 1998) involves the high latitudes, where large amount of heat is released by the ocean to the atmosphere, mostly in winter. This heat release is associated with the oceanic convection in winter that allows deep water to come at the surface and be cooled by air–sea fluxes, therefore releasing heat to the atmosphere. Consequently, a decrease in oceanic convection will reduce this heat transfer and will cool the atmosphere. Moreover, the associated decrease in deep water formation in one hemisphere can enhance deep water formation in the other, a process known as the bipolar ocean seesaw (BOS). Once more, these processes lead to a BCS pattern, that could explain the signal recorded in paleodata.

The two mechanisms described above to explain the BCS could both play a role when a freshwater input is released in the North Atlantic (NA), which reduces convection there (Broecker hypothesis), and weakens the AMOC and thus the cross-equatorial heat transport (Crowley hypothesis). Consequently, the triggering of the BCS by freshwater release in the NA appears to succeed in explaining paleodata (Schmittner et al. 2003; Knutti et al. 2004). The external forcing in such theories is the freshwater release in the NA, due to massive ice sheet melting there, whose causes are not well explained.

Nevertheless, since massive polar ice sheets are also found in Antarctica, freshwater input could also be released in the Southern Ocean (SO). Such freshwater releases seem to have actually occurred during the last de-glaciation (Kanfoush et al. 2000; Rohling et al. 2004; Philippon et al. 2006), with a potential impact on the AMOC (Weaver et al. 2003). The direct impact of SO freshwater release is firstly a reduction in the Antarctic Bottom Water (AABW) formation. This deep water occupies most of the bottom of the ocean and is consequently competing in the abyss with the North Atlantic Deep Water (NADW) formed in the NA, a mechanism already mentioned as the BOS. Modelling studies (Stocker et al. 1992; Seidov et al. 2001; Brix and Gerdes 2003) found that a decrease in AABW production leads to an increase in NADW production and conversely. Such a relationship is in agreement with the assumption of the theoretical box model of Rooth (1982) that relates the AMOC intensity with the density difference between deep water formed in both polar regions i.e. between NADW and AABW densities.

While the BCS relates the surface temperature of both hemispheres, the BOS is associated with deep water formation. Nevertheless, the BOS could generate the BCS as explained in Broecker's theory. This is notably why these two distinct phenomena have sometimes been put into one "general" bipolar seesaw. In this paper, we will make the distinction between the two seesaws and will focus on the BOS.

The BOS has also been invoked to explain paleo-ocean data from the Last Glacial Maximum (LGM), which show that the NADW cell was shallower than for present days (Duplessy et al. 1988). Modelling studies (Fichefet et al. 1994; Shin et al. 2003; Weber et al. 2007) suggested that an increase in the AABW production during the LGM could have lead the NADW cell to be shallower and less intense, in agreement with paleodata. In the future, potential global warming associated with massive anthropogenic greenhouse gas release could bring the West Antarctic ice sheet to melt, which could diminish the AABW formation and therefore stabilise the AMOC (Swingedouw et al. 2008) through the BOS.

Recently Seidov et al. (2005) questioned the validity (and simplicity) of the BOS. They showed, using an ocean−atmosphere coupled model, that a 1 Sv freshwater perturbation in the SO, south of 60°S during 100 years, does not lead to any increase in NADW formation. On the contrary, they found a slight decrease in the AMOC maximum after 100 years. They attribute this weakening in the AMOC to the spread of the freshwater input in the SO to all the oceanic basins, due to the intense Antarctic Circumpolar Current (ACC) that rapidly mixes water of the SO, and therefore propagates salinity anomalies. Seidov et al. (2005) argue that this effect was not present in their former ocean-only model experiments that were forced with fixed salinity anomalies in some key regions, like the Weddell and Ross Seas. Such an experimental design prevents AABW formation, but also the spread of salinity anomalies all over the ocean surface, due to the effect of restoring conditions at the surface. However, Seidov et al. (2005) noted their own experiments, which was still in transient phase, could not be strictly compared with the steady-state results of Seidov et al. (2001). Stouffer et al. (2007) using some of the simulations of Seidov et al. (2005) also insisted on the difference between freshwater release in the NA, where, due to continent configuration, the induced salinity anomalies stay confined in the neighbourhood of the area where it is dumped to the ocean, and freshwater release in the SO, where induced salinity anomalies can easily spread in other oceans.

Another process by which the SO could impact on the AMOC has been described by Toggweiler and Samuels (1995) and others (McDermott 1996; Gnanadesikan 1999; Brix and Gerdes 2003; Klinger et al. 2003). Toggweiler and Samuels show, using an OGCM with restoring boundary conditions, that the NADW formation rate is

mostly controlled in their model by the winds in the SH at the latitude of the Drake Passage. They called this process the "Drake Passage effect" and explain it by the fact that the northward Ekman drift at the Drake Passage latitudes, induced by surface winds, has to be balanced by a deep geostrophic current below the sill (2,300 m), i.e. the NADW export. Nonetheless, Rahmstorf and England (1997) contested this idea. They argued that the Ekman drift is not necessarily equilibrated by a deep interhemispheric current and can simply recirculate locally. Rahmstorf and England also shed light on the importance of using a coupled ocean–atmosphere model in order to account for the thermal negative feedback of the AMOC, which reduces its sensitivity to SO wind in their model. The "Drake Passage effect" nonetheless remains one potential forcing of the AMOC that still has to be taken into account when analysing the origin of AMOC changes associated with changes in SO forcing.

The existence of the BOS is thus under question, and the Seidov et al. (2005) and Stouffer et al. (2007) studies reveal that, if valid, the exact oceanic mechanisms by which this seesaw could operate remain unclear. They also put the stress on the importance of accounting for transient freshwater forcing, which are characteristic of ice sheet melting, and which could occur rather rapidly, e.g. in a few centuries (Chen et al. 1991; Bard et al. 1996).

The aim of this paper is twofold. Firstly, we will clarify the mechanisms and associated time scales at play in response to a freshwater release in the SO using an ocean–atmosphere coupled model. Secondly, we will analyse the importance of transient effects by evaluating the role of release rates of a given freshwater volume, mimicking different melting rates for the ice sheets in the SH. We aim at analysing the separate effects of wind, temperature and salinity changes in response to a SO freshwater input and to identify the associated oceanic mechanisms. For that purpose, we notably use a density binning analysis that helps to conciliate the dynamical and thermodynamical views of oceanic changes (Marshall et al. 1999). Moreover, we focus our study on time scales from years to centuries in order to understand in detail the time evolution of the system. This may help to better evaluate the transient oceanic response to a partial melting of the West Antarctic ice sheet for instance.

The paper is organised as follows. Firstly, we will describe the experimental design chosen to clarify the ocean and climate responses to a freshwater discharge in the SO (Sect. 2). Then, we will investigate the mechanisms and time scales of the different processes activated by this freshwater discharge (Sect. 3). We will further evaluate the impact of the freshwater discharge by analysing a large range of freshwater flux and durations (Sect. 4). Discussions and conclusions are given in the final section.

2 Experimental design

2.1 Model description

In this study, we use LOVECLIM1.1 (Driesschaert et al. 2007; Goosse et al. 2007), an Earth System Model of Intermediate Complexity (EMIC). LOVECLIM consists of five components representing the atmosphere (ECBilt), the ocean and sea ice (CLIO), the terrestrial biosphere (VECODE), the oceanic carbon cycle (LOCH) and the Greenland and Antarctic ice sheets (AGISM). Here we will not use the oceanic carbon cycle and ice sheet models since the focus will be on oceanic tunnels and atmospheric bridges (Liu and Alexander 2007) implied by the BOS.

ECBilt (Opsteegh et al. 1998) is a quasi-geostrophic atmospheric model with three levels and a T21 horizontal resolution, which contains a full hydrological cycle and explicitly computes synoptic variability associated with weather patterns. CLIO (Goosse and Fichefet 1999) is a primitive-equation, free-surface OGCM coupled to a thermodynamic-dynamic sea ice model. Its horizontal resolution is $3° \times 3°$, and there are 20 levels in the ocean. VECODE (Brovkin et al. 2002) is a reduced-form model of vegetation dynamics and of the terrestrial carbon cycle. It simulates the dynamics of two plant functional types (trees and grassland) at the same resolution as that of ECBilt. ECBilt–CLIO–VECODE has been utilised in a large number of climate studies (please refer to http://www.knmi.nl/onderzk/CKO/ecbilt-papers.html for a full list of references).

2.2 Numerical experiments

The different experiments performed in this study are summarised in Table 1. A first experiment (CTRL) has been integrated for 1,500 years under preindustrial climatic conditions and will be the control or reference simulation for the other experiments. This experiment starts after a spin-up of more than a thousand years, in order to reach a quasi-equilibrium state in the ocean. The second experiment (Hos1) begins from the same initial state and is similar to the Seidov et al. (2005) and Stouffer et al. (2007) "SO hosing" experiments: a 1 Sv ($1\ \text{Sv} = 10^6\ \text{m}^3/\text{s}$) freshwater flux is suddenly released (like an Heaviside step function) in the SO, south of 60°S, for 100 years. No salt compensation is applied in order to avoid any unexpected effects (Stocker et al. 2007). Moreover this choice is coherent with the aim of evaluating the effect of ice sheet meltwater pulses, which have no reason to be directly compensated in the real world. The freshwater perturbation is then suddenly removed and the experiment is continued for another 500 years without additional freshwater forcing. A third experiment (HosWind) is similar to Hos1 but surface wind stress is

Table 1 Description of the numerical experiments performed

Name of the experiment	Description
CTRL	1,500-year long control simulation under preindustrial conditions
Hos1	Sensitivity experiments where a 1 Sv freshwater input is added south of 60°S in the SO for 100 years, without any salt compensation in remote areas. The freshwater input is then stopped and the experiment is run for an additional 500 years
HosWind	Same experimental design as Hos1, except that the wind stress computed interactively by the atmospheric model to force the ocean is replaced at each time step by the daily varying values coming from the first 100 years of CTRL experiment. Those daily varying values, covering 100 years, are then used as many times as required by the simulation (i.e. 6 times here)
Hos0*i*	Sensitivity experiments where 0.*i* Sv freshwater input is added south of 60°S in the SO ($i \in \mathbb{N}$). The duration of the freshwater input is calculated as 1,000/*i* years. The freshwater input is then stopped and the experiments are run for an additional 500 years
Hos2	Same experiments as Hos1 but with a 2 Sv perturbation during 50 years

prescribed using the daily values of the first century of CTRL (which takes into account internal variability). This experiment without interactive wind stress is designed to test the potential effect of changes in wind stress induced by the climatic response to freshwater release in the SO. Additional "SO hosing" experiments have been performed in order to evaluate the role of the freshwater flux and duration. In all these sensitivity experiments, the same volume of freshwater is released in the SO: 3.11×10^{15} m^3, which represents approximately the volume of freshwater stored today above Greenland. We only modify the rate of the release and therefore the duration necessary for this release (see Table 1). For instance, Hos01 is an experiment where a 0.1 Sv freshwater flux has been released in the SO for 1,000 years, the simulation being then continued for another 500 years without freshwater perturbation, as in Hos1.

2.3 Density binning diagnosis

In order to properly quantify the changes in deep water masses (volume, production and export) induced by a freshwater release in the SO, we use the powerful diagnosis developed by Walin (1982) and Tziperman (1986) that quantifies the equilibrium between water mass formation and consumption by surface air–sea fluxes, diapycnal mixing and isopycnal export by the latitude–depth streamfunction (Fig. 1). This approach is a way to link dynamic and thermodynamic views of water mass transformation (Marshall et al. 1999).

This method can be sum up by the following equation (Speer et al. 2000; see Appendix):

$$\partial_t \mathcal{V} = -\Psi + \mathcal{F} + \mathcal{D} \quad (1)$$

where $\mathcal{V}$ is the volume within a control volume between two isopycnals ρ_1 and ρ_2, Ψ is the streamfunction transport at the northern and southern boundaries, counted positively when southward, $\mathcal{F}$ is the water mass formation by surface air–sea fluxes, and $\mathcal{D}$ is the formation by diapycnal mixing across the isopycnals ρ_1 and ρ_2 (Fig. 1). Note that the formation can be positive, which means that the volume $\mathcal{V}$ increases, while it decreases when the formation by air–sea fluxes or diapycnal mixing is negative.

In this paper, we define *deep water* as water denser or equal to 27.6 kg/m^3. This isopycnal is represented in Fig. 2, and approximately corresponds to the limit between the upper and the lower branches of the AMOC, which explains our choice. This choice is also in line with Schmitz (1996),

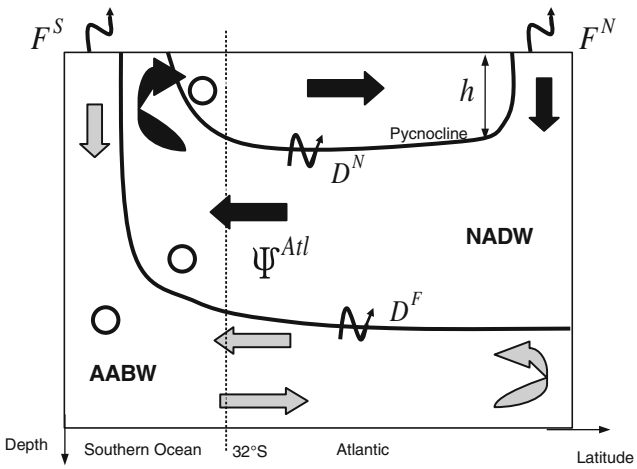

Fig. 1 Schematic view of a zonal mean of the Atlantic and Southern Oceans, dissociated at 32°S. Three different water masses are represented on this scheme. The upper layer, corresponding to the upper branch of the AMOC, is delimited by the pycnocline (as defined in Gnanadesikan et al. 2007) at the depth h. This pycnocline depth reaches 983 m in the Atlantic when averaged between 32°S and 40°N. We find that it matches closely the 27.6 kg/m^3 isopycnal in the different experiments (not shown). The second water mass represented is the NADW, which is mainly formed in the NA through air-sea interaction (F^N) and is exported to the other oceans at 32°S at a rate Ψ^{Atl}. This water mass is exchanged through diapycnal mixing with the upper layer (D^N) and with the AABW layer (D^F). The AABW is the third water mass represented here. It is formed in the SO at a rate F^S, reaches the bottom ocean, and notably goes in the Atlantic before coming back to the SO. The net volume transport of the AABW at 32°S is therefore equal to 0 in the Atlantic. The *circle* in the SO stands for water that turns around Antarctica and that can be exported in the Pacific or in the Indian Oceans

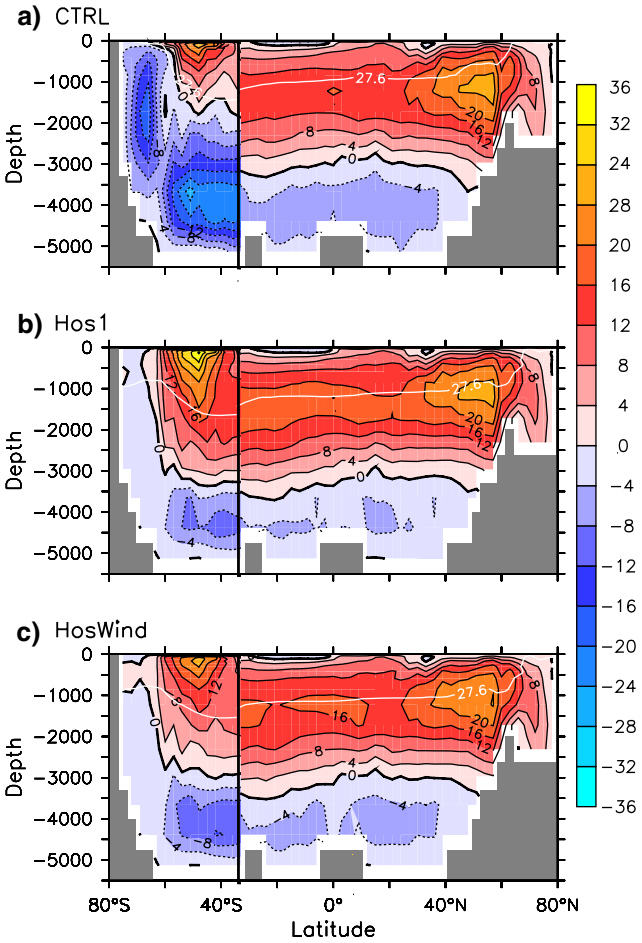

Fig. 2 Latitude-depth section of the meridional overturning streamfunction in the Atlantic Ocean (north of 32°S) and in the Southern Ocean (south of 32°S). *Red shading* denotes clockwise circulation and *blue* anticlockwise circulation. Are represented the first 100-year annual mean time averages from **a** CTRL, **b** Hos1, and **c** HosWind. The contour interval is 4 Sv. The 27.6 kg/m^3 zonally averaged isopycnal is superimposed in *white* in **a** and **b**

who defines NADW as water denser than 27.5 kg/m^3. In our model, NADW is however a bit denser than observation-based estimates, which explains the additional 0.1 kg/m^3 for our choice of deep water in the model. We then integrate Eq. 1 on the Atlantic basin, north of 32°S, and choose $\rho_1 = 27.6$ kg/m^3 and $\rho_2 = \infty$ (which means that we go down to the bottom of the ocean). This domain is called *North* and is identified by the superscript ^{N}. We therefore can rewrite Eq. 1 as:

$$\Psi^{Atl} = -\partial_t \mathcal{V}^N + \mathcal{F}^N + \mathcal{D}^N \quad (2)$$

The Bering Strait transport is here neglected since there is no water denser than 27.6 kg/m^3 that crosses it, so that Ψ^{Atl} stands for water denser than 27.6 kg/m^3 crossing the 32°S frontier. Since the AABW cell returns at depth, the net export of this water mass at the 32°S frontier is equal to 0, according to the scheme of Fig. 1 and the streamfunction of

Table 2 Different terms in the density binning analysis as described in Sect. 3

	Ψ_{Atl}	$-\partial_t \mathcal{V}^N$	$\mathcal{F}^N$	$\mathcal{D}^N$
CTRL	14.6	0.6	22.3	−8.6
HosWind–CTRL	2.4	4.1	−2.6	0.9
Hos1–HosWind	1.3	−0.1	1.3	0.1

These terms stand for a given water volume change $(-\partial_t \mathcal{V}^N)$ due to modifications in water formation and consumption by surface air–sea fluxes $(\mathcal{F}^N)$, diapycnal mixing $(\mathcal{D}^N)$ and isopycnal advection (Ψ^{Atl}). The exponent ^{N} stands for a three-dimensional integration on the *North* domain, north of 32°S in the Atlantic, and for density σ_0 larger or equal to 27.6 kg/m^3

Fig. 2a. The term Ψ^{Atl} therefore aims at representing the NADW export out of the Atlantic. In CTRL, Ψ^{Atl} equals 14.6 Sv when averaged over the first 100 years (Table 2), which is representative of the 14.0 Sv calculated as the maximum of the AMOC at 32°S (Fig. 2a). These figures are close to but a bit weaker than observation-based estimates from Talley (2003) who evaluate the NADW export at 32°S to be 17.8 Sv, fairly close to Ganachaud and Wunsch (2000) estimate of 16 Sv, obtained by using a different calculation. In CTRL, the formation of NADW $(\mathcal{F}^N)$ equals 22.6 Sv when averaged over the first 100 years, which is smaller than the 28.1 Sv of the AMOC maximum found around 50°N (Fig. 2a). This can be explained by the entrainment arising when NADW passes the Greenland–Iceland–Scotland Ridge, which enhances the AMOC intensity (Quadfasel and Kase 2007). Diapycnal mixing across the 27.6 kg/m^3 ispoycnal is equal to −8.6 Sv when averaged over the first 100 years of CTRL and represents the mixing of NADW with subsurface water above the isopycnal 27.6 kg/m^3. This isopycnal will be used in the following as a proxy of the pycnocline depth. The term $-\partial_t \mathcal{V}^N$ is small (0.6 Sv when averaged over the first 100 years) since CTRL experiment is close to equilibrium.

Equation 2 therefore succeeds in representing in a simple way the link between NADW formation by surface air–sea fluxes $(\mathcal{F}^N)$ and NADW export (Ψ^{Atl}), including the effect of diapycnal mixing with the upper ocean $(\mathcal{D}^N)$ and transient adjustment of water masses $(-\partial_t \mathcal{V}^N)$. It is therefore a very convenient method to diagnose the changes affecting the NADW cell in the sensitivity experiments, as shown below.

3 Mechanisms of oceanic adjustment to SO freshwater input

In this section, we will focus on the sensitivity experiments Hos1 and HosWind in order to evaluate the processes at

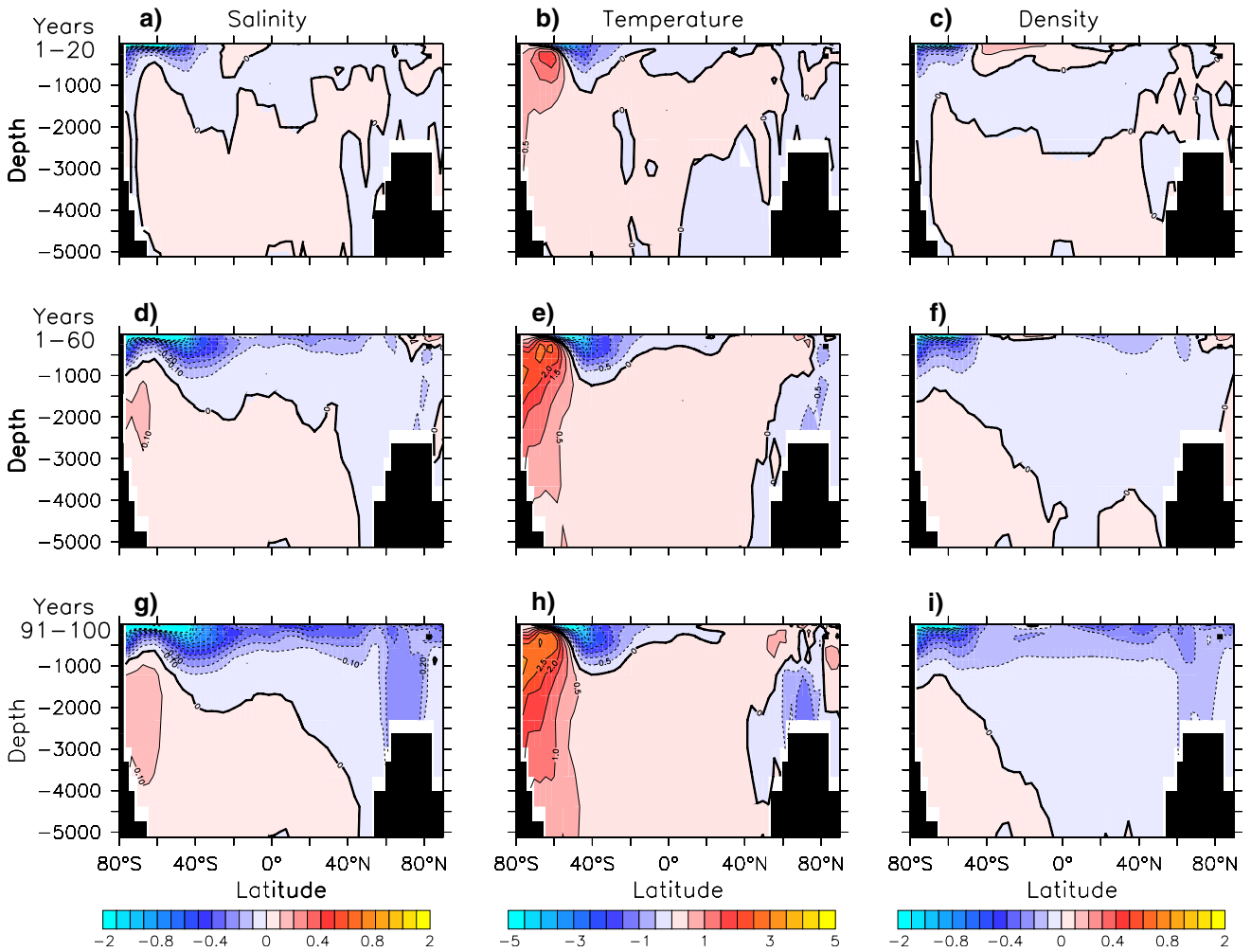

Fig. 3 Latitude–depth section of the difference between HosWind and CTRL (first 100-year annual mean) of the oceanic salinity (in PSU, *left column*), temperature (in °C, *middle column*) and density σ_0 (in kg/m^3, *right column*), zonally averaged over the whole ocean. The annual mean time averages over years 11–20 are in the first line, over years 51–60 in second line and over 91–100 in the third line

play in response to the freshwater hosing. Because of the freshwater released, the salinity decreases in the first hundred of meters of the ocean in HosWind compared to CTRL (Fig. 3, left column), mostly in the SO. This decrease in salinity reduces the vertical mixing in the SO and prevents convection in the Weddell and Ross Seas, so that the vertical transport is reduced. Since at high southern latitudes the deep ocean is warmer than the surface, this lack of convection in the SO leads to a cooling in the upper ocean and a warming in the deep ocean (Fig. 3, middle column). Note that the cooling at the surface partly compensates for the decrease in density due to the salinity decrease but not totally (Fig. 3, right column).

As a consequence of the lack of convection in the SO, the AABW cell weakens in Hos1 and HosWind by about 14 Sv (around 70% of CTRL value) in 40 years (Fig. 4a) and stabilises at the value of −6 Sv. After year 100 (when the freshwater release is over) it recovers in about five decades. In Hos1, the AMOC maximum slightly increases during the first 50 years and then decreases by about 8 Sv (about 25% of CTRL value, statistically significant at the 99% level by using a student test) in the next 50 years. From year 100, it slowly recovers and reaches its initial value around year 300. In HosWind the decrease in the AMOC maximum is a bit more pronounced, by around 1 Sv for the first 200 years.

The response of the AMOC maximum at 32°S is different from the one in the NA. It first increases by up to 4 Sv in Hos1 (around 30% of CTRL value, statistically significant at the 99% level by using a student test) in the first 20 years. It then stabilises around this enhanced value. Finally, it decreases at the end of the freshwater release (year 100), and, after an undershoot lasting around year 150, it reaches its initial value. In HosWind, the increase in the AMOC maximum at 32°S is similar, but is weaker by around 2 Sv.

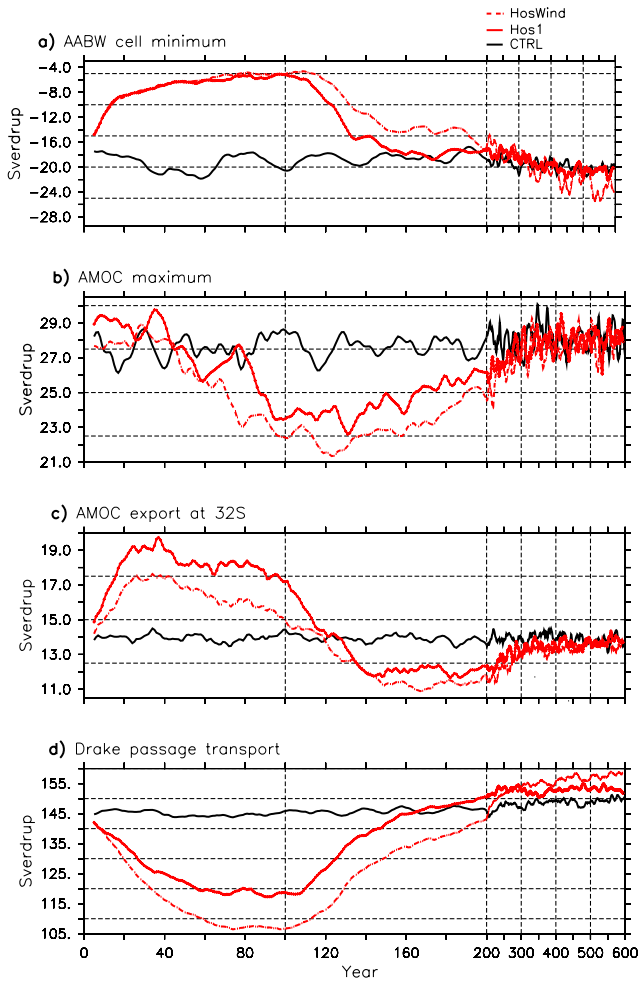

Fig. 4 Annual mean (in Sv) of: **a** the minimum value of the latitude–depth streamfunction in the SO south of 60°S, representing the AABW cell intensity; **b** the maximum value of latitude-depth streamfunction in the Atlantic, representing the NADW cell intensity; **c** the maximum value of latitude-depth streamfunction in the Atlantic at 32°S, representing the NADW export out of the Atlantic; **d** the volume of water transported through the Drake Passage, representing the intensity of the ACC. The *black line* represents CTRL, the *red line* Hos1 and the *red dashed line* HosWind. Note that the *horizontal scale* is stretched after year 200

This difference in the trend of these two AMOC indexes is illustrated in Fig. 5, left column, where a dipole pattern in latitude–depth section appears for the streamfunction difference between HosWind and CTRL. In the first decades, we observe a strengthening in the AMOC (Fig. 5a). After 50 years, a weakening of the AMOC happens in the northern part of the Atlantic basin (Fig. 5c). This weakening then propagates southward and concerns most of the Atlantic, north of the equator, after 100 years. South of the equator, the initial strengthening in the AMOC remains steady (Fig. 5e). In Fig. 5, right column, we also notice large differences for the latitude–depth streamfunction between Hos1 and HosWind: the streamfunction increases both in the SO and NA after a decade (Fig. 5b), illustrating a relative increase both in the Deacon and NADW cells when the wind changes are taken into account. This increase remains for the whole century (Fig. 5d, g).

To go further in depth in the analysis of the mechanisms explaining the AMOC response in Hos1 as compared to CTRL, we assume that the observed changes in the AMOC are caused by three different processes, whose effects can oppose each others. These processes are:

1. deep water adjustment;
2. salinity anomalies propagation;
3. southern wind increase.

In the following sub-sections, we will explain in details how these processes work. For this purpose, we isolate the role of processes 1 and 2 through the comparison of HosWind and CTRL and the influence of process 3 through the comparison of Hos1 and HosWind. We analyse the simulations using the binning approach (Sect. 2.3) as well as an evaluation of the north–south meridional gradient changes in the Atlantic. Based on scaling argument, this gradient is thought to be related with the AMOC (Rooth 1982; Rahmstorf 1996; Scott et al. 1999; Klinger and Marotzke 1999; Vallis 2000). For this purpose we use the mean density averaged over boxes in the northern and southern part of the Atlantic ocean (Fig. 6).

3.1 Deep water adjustment

The process that increases the NADW export at 32°S in HosWind is identified as the BOS effect. This mechanism has been explained as an oceanic adjustment in response to changes in deep water mass production i.e. an increase in the AABW production is associated with a decrease in NADW production and conversely. Here we use the density binning approach to clarify the processes and time scales governing this adjustment. In particular, we use the water mass balance summarised by Eq. 2 for deep water, which allows to relate water mass production with water mass export, diapycnal mixing and water mass volume adjustment. The importance of these different terms for the changes in export at 32°S in the Atlantic in HosWind as compared to CTRL are presented in Table 2. We notice an increase in NADW export at 32°S by about 2.4 Sv averaged over the first 100 years, which is in agreement with Fig. 4c. This increase appears to be mainly due to a 4.1 Sv decrease in deep water volume associated with the reduction in AABW production, and which leads to a deepening of the 27.6 kg/m^3 isopycnal. As shown in Fig. 7a, we also observe an increase in this isopycnal depth in the Atlantic. This deepening of the 27.6 kg/m^3 isopycnal propagates from 60°S to the equator in about one decade.

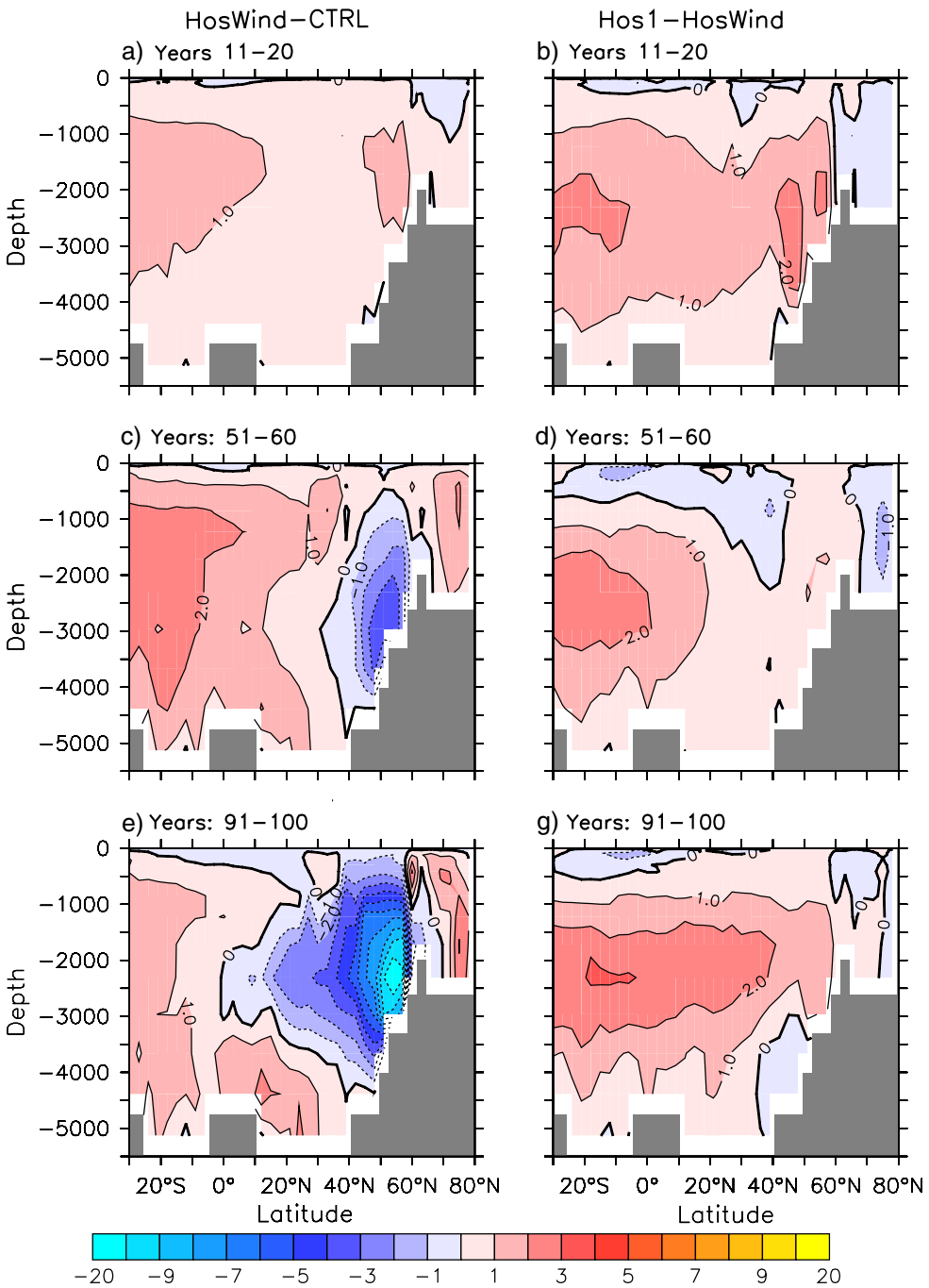

Fig. 5 Latitude–depth section of the meridional overturning streamfunction in the Atlantic Ocean (north of 32°S). *Red shading* denotes clockwise circulation and *blue* anticlockwise circulation. Are represented different snapshots for the differences between HosWind and CTRL (*left column*) and between Hos1 and HosWind (*right column*). The annual mean time averages over years 11–20 are in the first line, over years 51–60 on the second line, and over 91–100 on the third line. The contour interval is 2 Sv.

The adjustment of the 27.6 kg/m^3 isopycnal is so fast that it is very likely realised through oceanic waves propagation. Following Kawase (1987) arguments, confirmed by Johnson and Marshall (2002), we argue that buoyant anomalies, here located in the SO, affect the pycnocline depth and propagate northward as Kelvin waves along the western boundary region (i.e. South America in the Atlantic). At the equator, they cross zonally every basin, still as Kelvin waves, and then radiate Rossby waves, which propagate westward. From the equator, the adjustment also propagates northward and southward along the eastern boundary of each basin, through Kelvin waves. Oceanic wave trains excited by SO freshwater input has been observed in an OGCM by Hirschi et al. (2002). They notice that this wave propagation affects the oceanic large-scale dynamics and notably enhances the AMOC. As shown by Johnson and Marshall (2002), the equator may act as a low pass filter for the wave propagation and limit the northward propagation of the pycnocline anomalies (Fig. 7a).

The deepening of the 27.6 kg/m^3 isopycnal is associated with the decrease in AABW production. This deep water

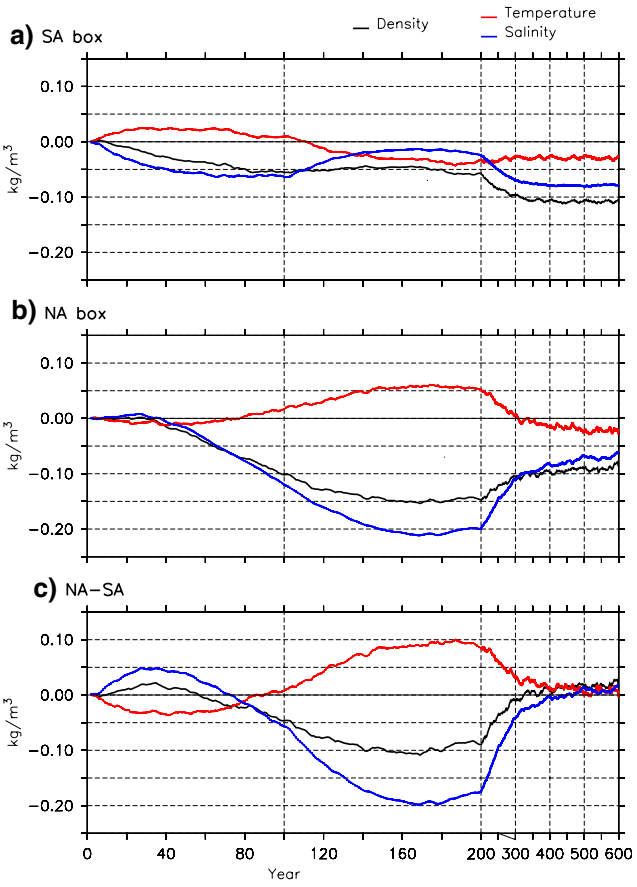

Fig. 6 Density differences between HosWind and CTRL in the: **a** SA box (between 50°S–30°S and 70°W–30°E), **b** NA box (between 50°S and 80°S, not including the Arctic basin) averaged in depth from the top to the bottom, and **c** the differences NA–SA, for the averaged density (*in black*), temperature (*red*) and salinity (*blue*) component for these density changes, under a linear assumption. This assumption has been checked and represents errors smaller than 1%. Note that the horizontal scale is stretched after year 200

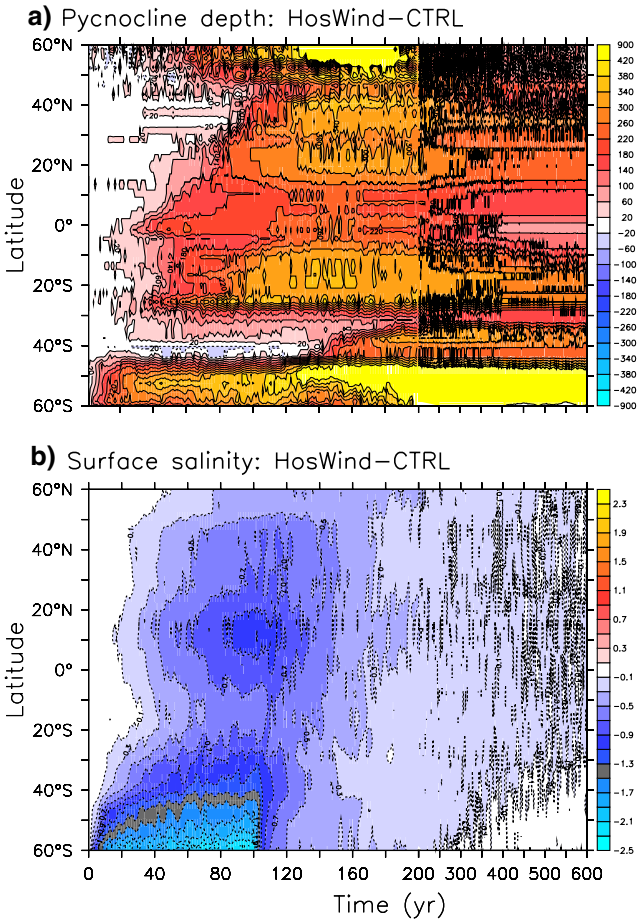

Fig. 7 Zonally averaged differences between HosWind and CTRL in the Atlantic basin of: **a** the 27.6 kg/m^3 isopycnal depth (in m); **b** the annual mean sea surface salinity (in PSU). *Blue shading* indicates negative values and *red shading* positive values. The contour interval is 40 m for **a** and 0.2 PSU for **b**. Note that the horizontal scale is stretched after year 200

mass is replaced by lighter water in the surface layers of the ocean, which deepens the 27.6 kg/m^3 isopycnal . This also affects the density and pressure structure of the whole water column. We notice on Fig. 6a that the density of the southern box diminishes very rapidly. If the density northward remains constant (which is true for the first 50 years as shown on Fig. 6b), this reduction increases the north–south density gradient leading to an enhancement of the AMOC coming from the south. This approach is coherent with the binning analysis and is another way of understanding how the process 1 enhances the AMOC from the south, as shown on Fig. 5a.

3.2 Salinity anomalies spread

After 50 years, we notice a decrease in density in the northern box in HosWind compared to CTRL (Fig. 6b). This reduction in density in the NA tends to diminish the north–south gradient of density. This decrease may therefore explain the weakening of the AMOC observed in the northern part of the basin. Moreover, we notice in Table 2 that the increase in NADW export at 32°S is attenuated by a 2.6 Sv decrease in NADW formation in HosWind compared to CTRL. This reduction is certainly due to the advective spread of salinity anomalies from the SO as described in Seidov et al. (2005). We see in Fig. 7b the northward propagation in the Atlantic of negative salinity anomalies coming from the SO, which reach 50°N in about 30 years, when a 0.1 PSU anomaly appears. The salinity anomalies reach 0.3 PSU around 50°N after 50 years. Consequently, the NADW formation anomaly (as defined in Eq. 2) in HosWind compared to CTRL becomes negative at that time (not shown), which explains the reduction in the AMOC maximum after 50 years (Fig. 4b).

The impact of process 1 and 2 may therefore both affect the AMOC maximum through changes in the north–south

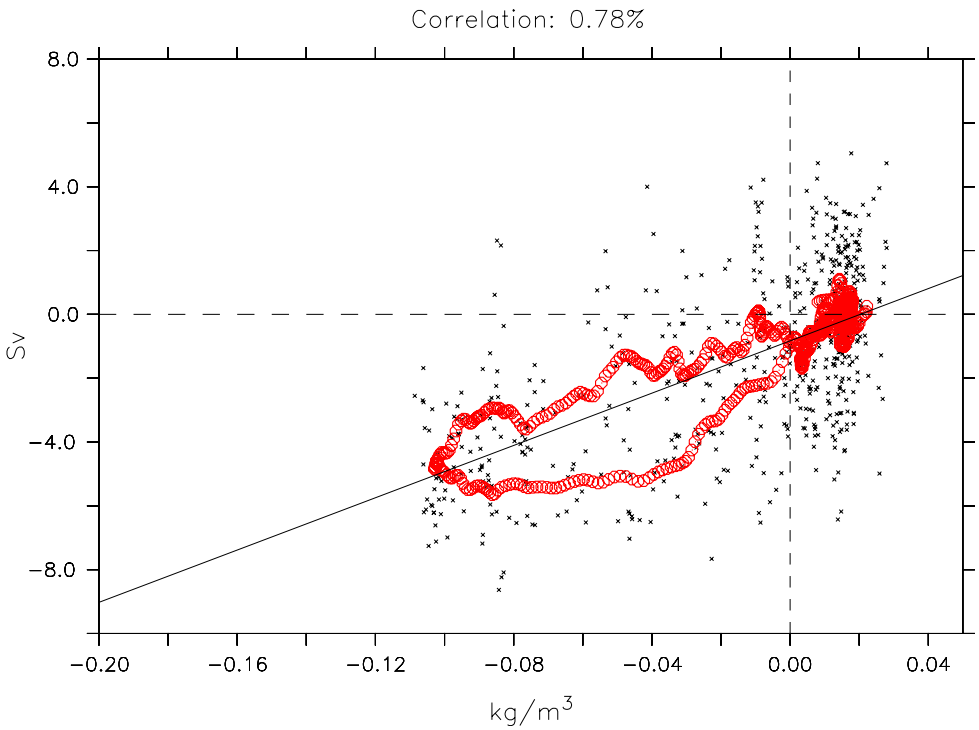

Fig. 8 Correlation of the differences in the AMOC maximum between HosWind and CTRL with the density differences averaged over two boxes located in the NA and the SA (see Fig. 6). The *black crosses* represent the annual mean for each year of the 600 years of the experiments. The *red circle* represents a 30-year running mean. The correlation for the 30-year running mean between density anomalies and AMOC maximum is of 0.78

density gradient from the north (process 2) or from the south (process 1). This assumption is supported by the 0.78 correlation between the AMOC maximum and the density differences of the northern minus southern boxes (Fig. 8). Different boxes have been tested, and the two boxes described in Fig. 6 exhibit the best correlation with the changes in the AMOC maximum. We use this relationship to evaluate the role played by changes in the SA and NA (Fig. 6c). We notice that most of the decrease in the density difference between the two boxes are explained by the density decrease in the NA box, while the changes in the SA box tends to damp this decrease. The temperature density component in the NA box also damps this decrease in agreement with the classical negative feedback related to the advection of temperature in the convection sites (e.g. Stommel 1961; Rahmstorf and England 1997; Swingedouw et al. 2007). We also notice that the recovery processes follow the changes in salinity in the NA box. The salinity anomaly there tends to increase after year 150 due to the stopping of the freshwater input in the SO (delayed by the transport of the anomaly in the NA) and the dilution of the salinity anomalies in the whole ocean. Finally, we notice that the density does not recover its initial value after 600 years in the NA and SA boxes (Fig. 6) contrary to the AMOC maximum. A 0.1 kg/m^3 mean density changes remains in both boxes. We also see this adjustment through the remaining deepening in 27.6 kg/m^3 isopycnal after 600 years (Fig. 7a). The ocean therefore almost recovers its initial state for the AMOC and north–south density gradient, but decreases its density both in the north and in the south, illustrating the dilution of salinity over the whole ocean.

3.3 Southern wind increase

The climatic impact of a freshwater input in the SO has been described in Stouffer et al. (2007) as a cooling in the SH and a slight warming in the NH. Here we obtain the same type of climatic impact, as seen in Fig. 9, since there is a 5°C cooling between Hos1 and CTRL averaged spatially south of 40°S for years 80–100, and a slight warming of about 1°C in the NA (statistically significant at the 99% level using a student test). The magnitude of the cooling simulated in our experiment is also similar to the study of Stouffer et al. (2007), showing that this result is not too sensitive to the atmospheric model. In fact, the SH cooling is mostly related to an increase in sea ice cover and its associated albedo feedback, in response to the lack of convection in the SO.

The SH cooling increases the meridional temperature gradient between the equator and Antarctica. In response to this change, the zonal wind increases in the SH high latitudes, as shown in Fig. 9. This increase activates the "Drake Passage effect", which explains why the NADW export at 32°S is 1.3 Sv stronger in Hos1 than in HosWind (Table 2). The NADW cell is strengthened over the whole Atlantic basin as shown in Fig. 2d, which stands for the impact of wind stress changes associated with the "SO hosing". We assume that these changes are mainly due to the wind stress increase in Hos1 compared to CTRL and

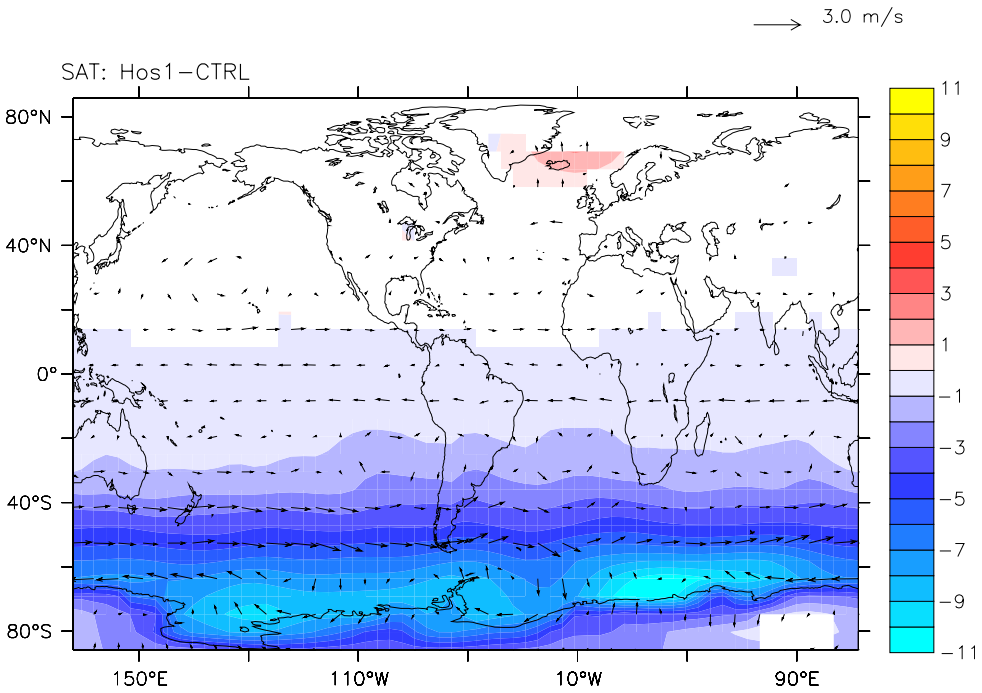

Fig. 9 Difference in Surface Air Temperature (SAT) averaged over the last 20 years of the experiments Hos1 and CTRL. The contour interval is 1°C and the *colored zones* correspond to the 99% student test significant differences. The wind speed (in m/s) differences are also represented in overlay (99% student test significant differences). The scale of the vector is given on the *upper right corner* of the figure

HosWind, around the latitudes of the Drake Passage, because it is the region where the changes are the largest (Fig. 9). Between 45 and 60°S, the zonal wind stress increases by 40% during the first 20 years and stabilises around this increased value up to year 100 (not shown).

The impact of the wind stress increase is also seen in water mass equilibrium from Eq. 2 (Table 2). NADW formation by air–sea fluxes is increased by 1.3 Sv in Hos1 compared to HosWind when averaged over the first 100 years. This indicates that the increase in NADW export at 32°S due to wind stress increase is associated with an increase in NADW formation of the same amount when comparing Hos1 and HosWind. This is due to the increased volume transport into the Atlantic that moves across the equator up to the NA, where it contributes to intensify the deep water formation and sinking.

Nonetheless, the increase in wind stress does not lead in the first century to any increase in the ACC transport, which decreases in Hos1 (Fig. 4d). This weakening of the ACC is due to a decrease in the meridional density gradient in the SO between 45°S and 60°S by around 45% (going from 110 to 60 g/m^3/°Lat.), due to the freshwater flux in the SO. This yields a decrease in the ACC through geostrophy, which dominates over the effect of wind stress increase.

4 Role of the freshwater flux amplitude

We now analyse the importance of the freshwater flux amplitude. The aim is to evaluate the response of the AMOC and climate when the freshwater release is delivered more slowly (but on a longer time scale) or more rapidly (but on a smaller time scale) . We define the *perturbation duration* (τ, expressed in years) as the duration of the freshwater input. τ is related to the freshwater flux (r), since the total volume of freshwater released is fixed to 100 Sv.yr in the different "SO hosing" experiments performed (see Table 1).

4.1 Ocean circulation

Figure 10 shows the time evolution of the response of chosen oceanic indexes to different freshwater fluxes. The qualitative picture for these experiments follows the general behaviour of Hos1, with a decrease in the absolute AABW maximum (Fig. 10a), a decrease in the NADW maximum (Fig. 10b), an increase in the NADW export (Fig. 10c) and a decrease in the ACC transport (Fig. 10d). We notice that the smaller the freshwater flux, the smaller the changes in the oceanic indexes. When the freshwater input is removed, we remark an overshoot or an undershoot for most of the indexes and simulations. In the following, we will try to understand how the deep oceanic circulation responds to different freshwater fluxes. For this purpose, we have performed in total 12 "SO hosing" experiments, creating a range of simulations with perturbation duration ranging from 50 to 1,500 years, with an associated freshwater flux ranging from 2 to 0.0667 Sv, respectively.

First of all, we observe that the AABW maximum, averaged over the whole perturbation duration, evolves like

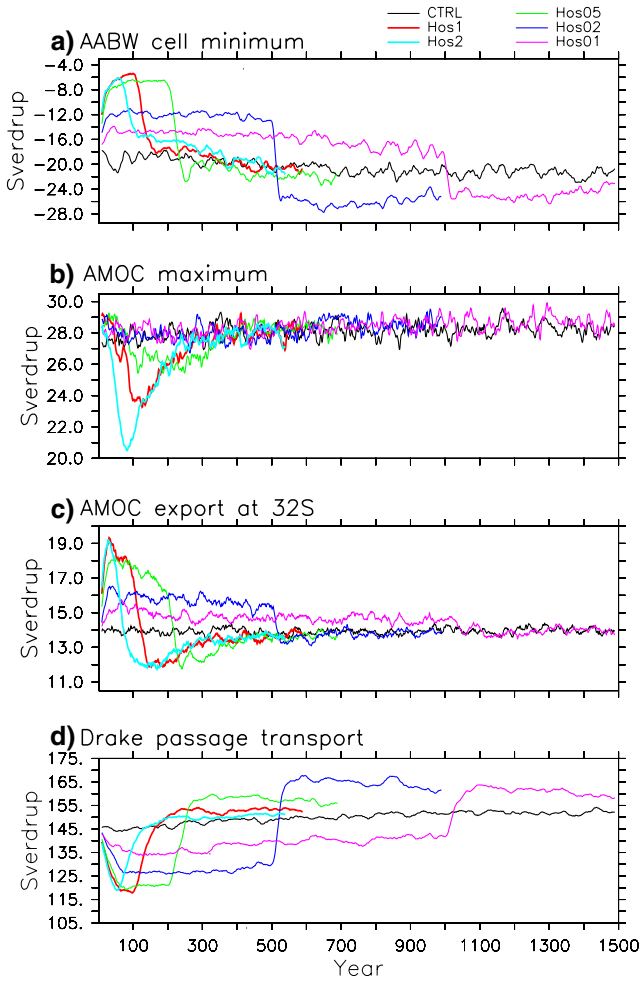

Fig. 10 Same figure as Fig. 4, but for additional "SO hosing" experiments. The *black line* represents CTRL, the *red line* Hos1, the *green line* Hos05, the *blue line* Hos02, the *purple line* Hos01 and the *cyan line* Hos2

the function $f(r) = K(1 - e^{-r/r_0})$ (Fig. 11a) where K is the saturation of the AABW weakening, which is around 12 Sv, illustrating the collapse of the AABW cell in that case. The e-folding r_0 of the exponential is found to be 0.2 Sv, which means that for $r = 3r_0 = 0.6$ Sv the AABW weakening equals 95% of the saturation value. The shape of the dependency of the AMOC export with the perturbation flux (Fig. 11b) is similar to the one of the AABW, but with a saturation of around 4 Sv of increase and an e-folding of 0.3 Sv. We interpret this increase in AMOC export as the impact of processes 1 and 3, damped by the impact of process 2. However, the latter never dominates for the export since we never obtain any decrease in the export. The AMOC maximum response against the perturbation flux is different from the two previous. We see in Fig. 11c that the AMOC maximum evolves linearly with the perturbation flux, which means that the larger the perturbation flux, the larger the AMOC maximum decrease. We also notice that for a perturbation flux smaller than 0.2 Sv, the AMOC maximum anomaly almost equals 0. This could be explained by the fact that processes 1 and 3 exactly compensate the effect of process 2 in this part of the phase space.

We also notice that the sea surface salinity (SSS) in the SO also evolves linearly with perturbation flux (Fig. 11d). This shows that the AMOC maximum change mainly occurs in the NA, and is mostly affected by process 2, which is dependent on the SSS anomaly spread from the south. It seems that if the SSS anomaly in the SO is weaker than 0.2 PSU, its transport toward the NA is not very efficient since part of this anomaly will be diluted during the journey. We therefore argue that the saturation for the AMOC maximum observed in Fig. 11c is mainly due to the slightness of the SSS anomaly in the SO for perturbation smaller than 0.2 Sv. For such a flux, the SSS anomalies are diluted in depth through the mean current and hardly affect the surface salinity in the NA, and their small impact is largely compensated by the effect of process 1 and 3.

4.2 Climatic impact

We now explore the sensitivity of the climate response to the freshwater release in the SO, already described in Fig. 9. Figure 12 indicates that the global heat transport at the end of the freshwater input is affected by the freshwater discharge duration. In the SH, we see that the faster the freshwater is released, the larger the southward heat transport is reduced. In the NH, the picture is not as clear for the relationship between heat transport and freshwater input duration. The northward heat transport increases in all the sensitivity experiments represented in Fig. 12, by as much as 0.24 PW and 0.11 PW at 20°N in Hos2 and Hos1, respectively, when compared to CTRL. The increase in Hos05 is very similar to Hos02 and Hos01. This heat transport response clearly allows the development of a BCS as shown in Fig. 9 with larger amplitude for temperature differences in the SH than in the NH, as noticed by Stouffer et al. (2007).

The influence of the freshwater flux on the SH climate is represented in Fig. 13. The decrease in Surface Air Temperature (SAT), south of 40°S and averaged over the whole freshwater duration (Fig. 13a), diminishes exponentially with the increase in perturbation flux, with an e-folding of around 0.2 Sv as for the AABW weakening. It saturates at −5.1°C. Both the global southward oceanic heat transport anomalies at 30°S (Fig. 13b) and the sea ice cover anomalies in the SH also decrease exponentially with the perturbation flux with the same e-folding and a saturation of 0.28 PW and 11.5 × $10^6 m^2$, respectively. These changes in sea ice cover are associated with changes in mixed layer depth (MLD) in the SO. We see in Fig. 13d that the

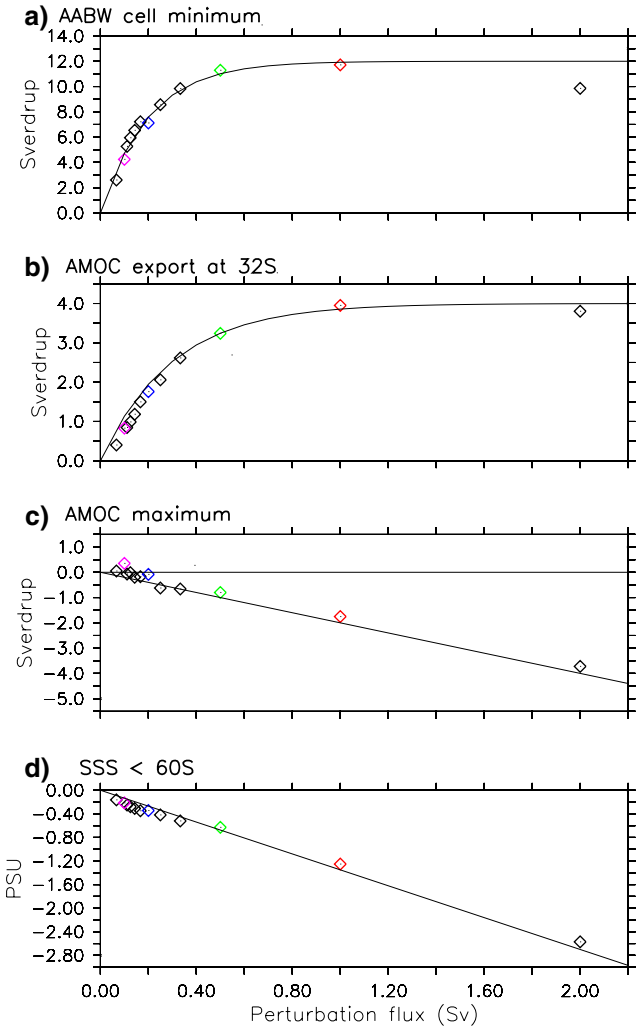

Fig. 11 Diagram of different ocean index differences with CTRL (already defined in Fig. 4) against the perturbation flux (in Sv) for **a** the AABW cell intensity (in Sv); **b** the AMOC export at 32°S (in Sv); **c** the AMOC maximum (in Sv); **d** the sea surface salinity (SSS) in the SO south of 60°S (in PSU). In **a**, **b** and **d**, the indexes have been averaged over the freshwater perturbation duration, and in **c** the freshwater perturbation duration plus 30 years after the end of the freshwater perturbation, in the different sensitivity experiments. This last period has been chosen in order to account for the lag of around 30 years for the salinity anomalies to reach the NA convection sites and affect the NADW cell. The *red square* represents Hos1, the *green square* Hos05, the *blue square* Hos02, the *purple square* Hos01 and the *cyan square* Hos2. A linear or exponential regression are plotted over each panels in *thin black lines*

negative anomaly of the MLD in the SO increases exponentially with perturbation flux with a faster *e*-folding of 0.15 Sv (meaning that MLD is more sensitive than the other indexes to freshwater input), and saturates at around −32 m.

The evolution of the four first climatic indexes represented in Fig. 13 therefore seems to be related with each other. In particular, SAT and sea ice cover changes exhibit

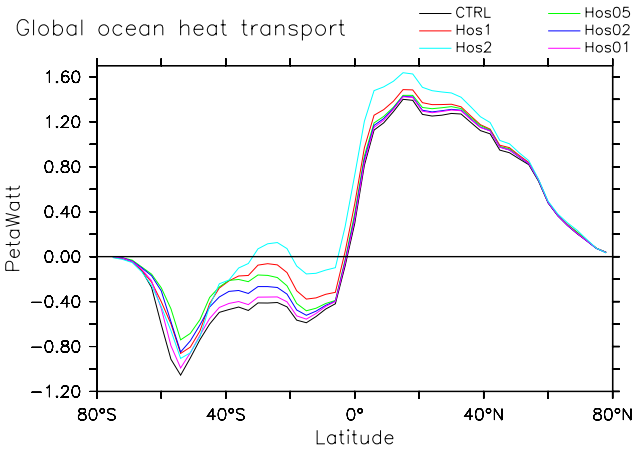

Fig. 12 Global northward ocean heat transport (PW) averaged over the last 20 years of the whole freshwater perturbation duration for the different experiments. The *black line* represents CTRL, the *red line* Hos1, the *green line* Hos05, the *blue line* Hos02, the *purple line* Hos01 and the *cyan line* Hos2

a similar sensitivity to the perturbation duration but with an opposite evolution (increase in sea ice cover corresponds to decrease in SAT). We conclude that the mechanisms to explain the SAT decrease in our model are similar to the ones proposed by Stouffer et al. (2007): the freshwater input in the SO shallows the mixed layer there and diminishes the vertical oceanic mixing with the deep ocean layer and reduces southward heat transport in the SH, so that the cooling of surface water by the atmosphere is faster, which leads to an increase in sea ice cover. This increases the surface albedo and strongly cools the surface. Finally, we notice that the changes in surface temperature are associated with changes in zonal wind south of 40°S (Fig. 13d), that also increase exponentially with perturbation flux with a large *e*-folding of 0.35 Sv and a saturation of 0.46 m/s. Due to this large *e*-folding, the process 3 will therefore affects the AMOC for larger perturbation flux than process 1.

5 Discussions and conclusions

In this study, we have analysed the impact of a freshwater input in the Southern Ocean. We have put the focus on the transient response to freshwater input as well as on the different effects produced by wind, temperature and salinity changes and the associated mechanisms. The use of different sensitivity experiments and diagnoses (water mass binning and north–south density gradient) have allowed us to identify three main processes that affect the AMOC in response to a SO freshwater input:

1. The deep water adjustment tends to intensify the NADW cell (mostly its export out of the Atlantic

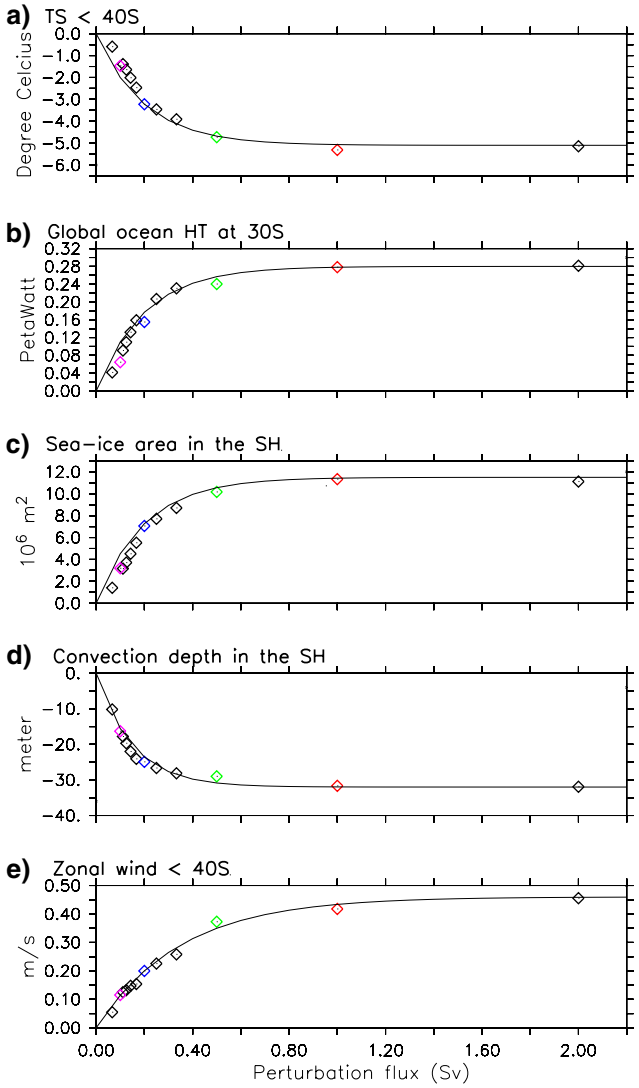

Fig. 13 Diagram of different climate index differences against the perturbation flux (in Sv) averaged over the freshwater perturbation minus CTRL (averaged on the same time). **a** Surface air temperature averaged south of 40°S (in °C). **b** Global ocean heat transport at 30°S (in PW). **c** Sea ice thickness in the Southern Hemisphere (in m). **d** mixed layer depth south of 60°S (in m). **e** Mean zonal wind speed south of 40°S (in m/s). The *red square* represents Hos1, the *green square* Hos05, the *blue square* Hos02, the *purple square* Hos01 and the *cyan square* Hos2. An exponential regression are plotted over each panels in *thin black lines*

around 32°S), one decade after the beginning of the freshwater input, through the decrease in density in the SO, associated with a deepening of the Atlantic pycnocline in response to the freshwater input and AABW production decrease. We have considered this process as being the so-called BOS (Stocker et al. 1992).

2. The spread of salinity anomalies from the SO up to the NA tends to weaken the NADW cell (mostly its maximum around 50°N), five decades after the beginning of the freshwater input, because it decreases the NADW production in the NA convection sites, an effect damped by changes in temperature and salinity elsewhere in the Atlantic basin. This process is similar to the one identified in the Seidov et al. (2005) and Stouffer et al. (2007) experiments, but is here clarified.
3. The SH wind increase, in response to the cooling in the SH that increases the SH meridional SAT gradient, tends to strengthen the NADW cell, one decade after the beginning of the freshwater input, through the "Drake Passage effect". This process is therefore related to ocean–atmosphere interactions, and has not been reported yet in other "SO hosing" experiments.

Processes 1 and 3 enhance the AMOC and tend to counteract the effect of process 2. Moreover, these three processes exhibit different characteristic time scales so that their effects are not efficient exactly at the same time.

We have also analysed the effect of different freshwater release rates and durations for the response of the AMOC. We have kept the same freshwater amount released in the SO (100 Sv.yr) but we have modified the perturbation flux (and duration) for this release. This was done to mimic the freshwater release by a given ice sheet, and to test the importance of its melt speed. This is justified by the uncertainty concerning ice sheet dynamics and future melting (Alley et al. 2005). We have shown in different "SO hosing" experiments that AABW, SO winds and NADW export anomalies evolve as an exponential with the perturbation flux. This is in contrast with the changes in AMOC maximum that evolve linearly with the perturbation flux. We have explained this difference of sensitivity to freshwater flux between AMOC maximum and NADW export by the fact that process 1 and 3 mostly affect the NADW export and are influenced by AABW and wind stress changes (respectively), while process 2 mostly affects the AMOC maximum and follows the spread of SSS anomalies from the SO. These SSS anomalies in the SO also evolves linearly with perturbation flux, an effect which explains the AMOC maximum sensitivity. We find that a freshwater flux larger than 0.2 Sv leads to the dominance of process 2 and a decrease of the AMOC maximum, while the NADW export remains enhanced by processes 1 and 3.

Lastly, we have analysed the climatic impact associated with a freshwater release in the SO. At the end of the freshwater perturbation, we find an important SH cooling of up to 5°C when averaged south of 40°N, which decreases exponentially with the perturbation flux with a similar *e*-folding of 0.2 Sv than AABW changes. This shows that the faster the freshwater flux is, the larger the SH is cooled. This effect is related to an increase in sea ice cover in response to the freshwater release in the SO due to a decrease in southward heat transport in the SH and a shallowing of the

MLD in the SO, both indexes that also evolve exponentially with perturbation flux, with similar *e*-foldings.

Our results are compatible with the Seidov et al. (2005) and Stouffer et al. (2007) "SO hosing" experiments. These two studies put the stress on the existence of process 2. In the present study, we clarify the intensity of the different processes involved in "SO hosing" experiments. We also find a new process (increase in SH winds) related to an ocean–atmosphere interaction, which can only be found in coupled ocean–atmosphere models. Moreover, we have enlightened the way the BOS (process 1) works: it is associated with a fast pycnocline adjustment in response to the decrease in deep water production in the SO, and likely caused by a wave propagation in the Atlantic basin. Consequently, this process has a characteristic time scale of a few years. It is therefore not controlled by the diapycnal mixing time scale as hypothesised by Broecker (1998). This type of enhancement of the AMOC through changes in the pycnocline is consistent with Gnanadesikan (1999) analysis. He showed with a simple analytical model that deepening the pycnocline in the Atlantic enhances the volume transport of the upper branch of the AMOC and therefore increases the sinking in the NA and the whole AMOC.

Weaver et al. (2003) found that a large freshening (up to 1 Sv) of the SO can enhance the AMOC. However, this result was obtained for an off state of the AMOC, with no deep water formation in the NA., which is not the case in our study. This result does not contradict our conclusion but shows that our study applies for a present-day active mode of the AMOC. Trevena et al. (2008) using the same model as Weaver et al. (the UVic model) showed that a large freshening of the SO can lead to a collapse of a glacial active AMOC and also weaken a present-day active AMOC. This stresses the importance of the state of the AMOC when analysing the impact of a freshwater input in the SO. Given the freshwater volume released in Trevena et al. (around 280 Sv.yr applied during 500 years, or a mean flux larger than 0.2 Sv), we can argue that the leading mechanism for the AMOC maximum in their experiment is our so-called process 2, which explains the weakening of the AMOC found in their experiment.

Our results underline the importance of the freshwater release fluxes. SO freshwater fluxes are not very well constrained in paleodata. A modelling study of the last deglaciation suggests an Antarctic ice sheet melting rate of about 0.03 Sv (Philippon et al. 2006). According to the present study, such a rate may have very little impact in terms of SH climate and BOS. Nonetheless, in millennial climate change projections, Swingedouw et al. (2008) found a rate of 0.14 Sv for the Antarctic ice sheet melting after 3,000 years of 4 × CO_2 stabilisation. They found that accounting for such a melting for the Antarctic ice sheet reduces the AMOC weakening. Considering the results from the present study, we argue that this effect is due to processes 1 and 3 that may dominate over the effect of process 2 for this type of freshwater flux (Fig. 11).

Concerning the climatic impact of the SO freshwater input, we plead that the observed BCS in paleodata (Blunier and Brooke 2001; EPICA Community Members 2006), with a large and abrupt cooling in Greenland, associated with gradual and smaller amplitude warming in Antarctica, could not be explained by SO freshwater discharges. Such discharges will lead to a large cooling in Antarctica and a slight warming around Greenland. They may however modulate the classical BCS picture.

Our results will certainly gain confidence if verified by other ocean–atmosphere models. In particular, given the importance of freshwater input in the SO for the ocean and climate, we argue that the Antarctic ice sheet, which has the potential to generate large freshwater input in the future, has to be properly modelled and coupled to state-of-the-art climate models.

Acknowledgments We are grateful to two anonymous reviewers for helpful advice and comments. We thank the European Marie Curie Research Training Network for Ice sheet and Climate Evolution (NICE) for its support. We also acknowledge the ASTER (Assessment of modelling uncertainties in long-term climate and sea level change projections) and BELCANTO (BELgian research on Carbon uptake in the ANTarctic Ocean) projects funded by the Belgian Science Policy for their support. The authors wish to acknowledge use of the Ferret program for analysis and graphics in this paper and the help of Patrick Brockmann for the use of this program.

Appendix: Formation–diffusion equilibrium

In this appendix, we explain how to obtain the Eq. 1 and how to calculate the terms of this equation in the model.

Following Speer et al. (2000), we firstly calculate a density flux defined as:

$$f = -\frac{\alpha g Q}{\rho_0 C_p} + \frac{\rho(T,0)\beta S}{\rho_0(1-S)}E \tag{3}$$

where S is the surface salinity, T is the surface temperature, C_p is the specific heat of seawater, ρ is the density, E is the net freshwater fluxes, α is the thermal expansion coefficient and β the haline contraction coefficient.

From the buoyancy flux, we can define the *transformation* by air–sea fluxes from one density class to another:

$$\mathcal{T} = \int_T dt \int_{S_b} dxdyf\,\delta(\rho' - \rho) \tag{4}$$

Its derivative with respect to buoyancy ($b = -g\rho/\rho_0$) is called the *formation* ($\mathcal{F}$) and represents the amount of new formation of a given water mass by air-sea buoyancy flux on a period T.

$$\mathcal{F} = -\partial_b \mathcal{T} \tag{5}$$

We define $\mathcal{A}$ as the net advective flux across isopycnals:

$$\mathcal{A} = \int_{S_b} (\overrightarrow{V} \cdot \overrightarrow{n}) d\Sigma \tag{6}$$

where $d\Sigma$ is the isopycnal surface area, $\overrightarrow{V}$ is the velocity and $\overrightarrow{n}$ is the unity normal vector to isopycnal.

We define $\mathcal{M}$ as the mixing or diffusive flux across isopycnals:

$$\mathcal{M} = \int_{S_b} -\kappa \partial_n b d\Sigma \tag{7}$$

where κ is the diapycnal diffusivity.

Ignoring volume fluxes across the sea floor and the sea surface, volume and mass conservation then write respectively:

$$\partial_t \delta v = (-\partial_b \mathcal{A} - \partial_b \psi^c)\delta b \tag{8}$$

$$\partial_t \delta (vb) = (-\partial_b (\mathcal{A} b) - \partial_b \mathcal{M} - b\partial_b \psi^c)\delta b \tag{9}$$

where ψ^c is the streamfunction at the control surface. These equations give:

$$\mathcal{T} - \mathcal{A} - \partial_b \mathcal{M} = 0 \tag{10}$$

Lastly, we eliminate advection $\mathcal{A}$ to obtain the volume balance of the isopycnal b (Speer et al. 2000) given by Eq. 11:

$$\partial_t V_b = -\partial_b \psi^c - \partial_b \mathcal{T} + \partial_{b^2} \mathcal{M} \tag{11}$$

which allows to define the diapycnal mixing term as $\mathcal{D} = \partial_{b^2} \mathcal{M}$ and the streamfunction export term as $\Psi = \partial_b \psi^c$. With this notation, we obtain the Eq. 1.

We calculate the different terms of Eq. 1 (Table 2) for different numerical experiments using $\delta\rho = 0.05$ kg/m^3 with monthly mean output for the different oceanic variables, which is precise enough according to the analysis from Speer et al. (2000).

References

Alley RB, Clark PU, Huybrechts P, Joughin I (2005) Ice-sheet and sea-level changes. Science 310:456–460

Bard E, Hamelin B, Arnold M, Montaggioni L, Cabiochparallel G, Faure G, Rougerie F (1996) Deglacial sea-level record from Tahiti corals and the timing of global meltwater discharge. Nature 382:241–244

Blunier T, Brook EJ (2001) Timing of millennial-scale climate change in Antarctica and Greenland during the last glacial period. Science 291:109–112

Broecker WS (1998) Paleocean circulation during the last deglaciation: a bipolar seesaw? Paleoceanography 13:119–121

Brovkin V, Bendtsen J, Claussen M, Ganopolski A, Kubatzki C, Petoukhov V, Andreev A (2002) Carbon cycle, vegetation, and climate dynamics in the Holocene: experiments with the CLIMBER-2 model. Global Biogeochem Cycles 16:GB001662

Brix H, Gerdes R (2003) Influence of high-latitude surface forcing on the global thermohaline circulation. J Geophys Res 108:Art. no. 3022

Chen JH, Curran HA, White B, Wasserburg GJ (1991) Precise chronology of the Last Interglacial Period: U-234-Th-230 data from fossil coral reefs in the Bahamas. Geol Soc Am Bull 103:82–97

Crowley TJ (1992) North Atlantic deep waters cools the Southern Hemisphere. Paleoceanography 7:489–497

Driesschaert E, Fichefet T, Goosse H, Huybrechts P, Janssens I, Mouchet A, Munhoven G, Brovkin V, Weber SL (2007) Modelling the influence of Greenland ice sheet melting on the Atlantic meridional overturning circulation during the next millennia. Geophys Res Lett 34:L1070

Duplessy JC, Shackleton NJ, Fairbanks R, Labeyrie L, Oppo D, Kallel N (1988) Deep water source variation during the last climatic cycle and their impact on the global deep water circulation. Paleoceanography 3:343–360

EPICA Community Members (2006) One-to-one coupling of glacial climate variability in Greenland and Antarctica. Nature 444:195–198

Fichefet T, Hovine S, Duplessy J-C (1994) A model study of the Atlantic thermohaline circulation during the last glacial maximum. Nature 372:252–255

Ganachaud A, Wunsch C (2000) Improved estimates of global ocean circulation, heat transport and mixing from hydrographic data. Nature 408:453–457

Gnanadesikan A (1999) A simple predictive model for the structure of the oceanic pycnocline. Science 283:2077–2079

Gnanadesikan A, de Boer AM, Mignone BK (2007) A simple theory of the pycnocline and overturning revisited. In: Schmittner A, Chiang JCH, Hemming SR (eds) Ocean circulation: mechanisms and impacts, AGU monograph, Washington, pp 19–32

Goosse H, Fichefet T (1999) Importance of ice–ocean interactions for the global ocean circulation: a model study. J Geophys Res 104:337–355

Goosse H, Driesschaert E, Fichefet T, Loutre M-F (2007) Information on the early holocene climate constrains the summer sea ice projections for the 21st century. Clim Past 3:683–692

Hirschi J, Stocker TF (2002) Rapid changes of the oceanic circulation in a hierarchy of ocean models. Tellus A 54A:273–287

Johnson HL, Marshall DP (2002) A theory for the surface Atlantic response to thermohaline variability. J Phys Oceanogr 32:1121–1132

Kanfoush SL, Hodell DA, Charles CD, Guilderson TP, Mortyn PG, Ninnemann US (2000) Millennial-scale instability of the Antarctic ice sheet during the last glaciation. Science 288:1815–1818

Kawase M (1987) Establishment of deep ocean circulation driven by deep-water production. J Phys Oceanogr 17:2294–2317

Klinger BA Marotzke J (1999) Behavior of double-hemisphere thermohaline flows in a single basin. J Phys Oceanogr 29:382–399

Klinger BA, Drijfhout S, Marotzke J, Scott J (2003) Sensitivity of basin-wide meridional overturning to diapycnal diffusion and remote wind forcing in an idealized Atlantic–Southern Ocean geometry. J Phys Oceanogr 33:249–266

Knutti R, Fluckiger J, Stocker TF, Timmermann A (2004) Strong hemispheric coupling of glacial climate through freshwater discharge and ocean circulation. Nature 430:851–856

Liu Z, Alexander M (2007) Atmospheric bridge, oceanic tunnel, and global climatic teleconnections. Rev Geophys 45:RG000172

Marshall J, Jamous D, Nilsson J (1999) Reconciling thermodynamic and dynamic methods of computation of water-mass transformation rates. Deep Sea Res 46:545–572

McDermott DA (1996) The regulation of northern overturning by southern hemisphere winds. J Phys Oceanogr 26:1234–1255

Opsteegh JD, Haarsma RJ, Selten FM, Kattenberg A (1998) ECBILT: a dynamic alternative to mixed boundary conditions in ocean models. Tellus A 50:348–367

Philippon G, Ramstein G, Charbit S, Kageyama M, Ritz C, Dumas C (2006) Evolution of the Antarctic ice sheet throughout the last deglaciation: a study with a new coupled climate—north and south hemisphere ice sheet model. Earth Planet Sci Lett 248:750–758

Quadfasel D, Kase R (2007) Present-day manifestation of Nordic Seas outflows. In: Schmittner A, Chiang JCH, Hemming SR (eds) Ocean circulation: mechanisms and impacts, AGU monograph, Washington, pp 75–90

Rahmstorf S (1996) On the freshwater forcing and transport of the Atlantic thermohaline circulation. Clim Dyn 12:799–811

Rahmstorf S, England MH (1997) Influence of southern hemisphere winds on North Atlantic deep water flow. J Phys Oceanogr 27:2040–2054

Rohling EJ, Marsh R, Wells NC, Siddall M, Edwards NR (2004) Similar meltwater contributions to glacial sea level changes from Antarctic and northern ice sheets. Nature 430:1016–1021

Rooth C (1982) Hydrology and ocean circulation. Prog Oceanogr 11:131–149

Schmittner A, Saenko OA, Weaver AJ (2003) Coupling of the hemispheres in observations and simulations of glacial climate change. Quat Sci Rev 22:659–671

Schmitz WJ (1996) On the world ocean circulation, vol 1. Woods Hole Oceanographic Institute WHOI-96-03, p 141

Scott JR, Marotzke J, Stone PH (1999) Interhemispheric thermohaline circulation in a coupled box model. J Phys Oceanogr 29:351–365

Seidov D, Barron E, Haupt BJ (2001) Meltwater and the global ocean conveyor: northern versus southern connections. Glob Planet Change 30:257–270

Seidov D, Stouffer RJ, Haupt BJ (2005) Meltwater and the global ocean conveyor: northern versus southern connections. Glob Planet Change 49:19–27

Shin SI, Liu Z, Otto-Bliesner B, Brady EC, Kutzbach JE, Harrison SP (2003) A simulation of the last glacial maximum climate using the NCAR-CCSM. Clim Dyn 20:127–151

Speer K, Guilyardi E, Madec G (2000) Southern Ocean transformation in a coupled model with and without eddy mass fluxes. Tellus 52:554–565

Stocker TF, Wright DG, Broecker WS (1992) The influence of high-latitude surface forcing on the global thermohaline circulation. Paleoceanography 7:529–541

Stouffer RJ, Seidov D, Haupt BJ (2007) Climate response to external sources of freshwater: North Atlantic versus the Southern Ocean. J Clim 20:436–448

Stocker TF, Timmermann A, Renold M, Timm O (2007) Effects of salt compensation on the climate model response in simulations of large changes of the Atlantic meridional overturning circulation. J Clim 20:5912–5928

Stommel H (1961) Thermohaline convection with two stable regimes of flow. Tellus 13:224–230

Swingedouw D, Braconnot P, Delecluse P, Guilyardi E, Marti O (2007) Quantifying the AMOC feedbacks during a $2 \times CO_2$ stabilization experiment with land-ice melting. Clim Dyn 29:521–534

Swingedouw D, Fichefet T, Huybrechts P, Goosse H, Loutre MF (2008) Antarctic ice-sheet melting provides negative feedbacks on future global warming. Geophys Res Lett 35:Art. no L17705

Talley LD (2003) Shallow, intermediate, and deep overturning components of the global heat budget. J Phys Oceanogr 33:530–560

Toggweiler JR, Samuels B (1995) Effects of the westerly wind stress over the Southern Ocean on the meridional overturning. Deep Sea Res 42:477–500

Trevena J, Sijp WP, England MH (2008) North Atlantic deep water collapse triggered by a Southern Ocean meltwater pulse in a glacial climate state. Geophys Res Lett 35:L09704

Tziperman E (1986) On the role of interior mixing and air–sea fluxes in determining the stratification and circulation of the ocean. J Phys Oceanogr 16:680–693

Vallis GK (2000) Large-scale circulation and production of stratification: effects of wind, geometry, and diffusion. J Phys Oceanogr 30:933–954

Walin G (1982) On the relation between sea-surface heat flow and thermal circulation in the ocean. Tellus 34:187–195

Weaver AJ, Saenko OA, Clark PU, Mitrovica JX (2003) Meltwater pulse 1A from Antarctica as a trigger of the Bolling-Allerod warm interval. Science 299:1709–1713

Weber SL, Drijfhout SS, Abe-Ouchi A, Crucifix M, Eby M, Ganopolski A, Murakami S, Otto-Bliesner B, Peltier WR (2007) The modern and glacial overturning circulation in the Atlantic Ocean in PMIP coupled model simulations. Clim Past 3:51–64